Composite Structures 94 (2012) 1861–1870

Contents lists available at SciVerse ScienceDirect

Composite Structures

journal homepage: www.elsevier.com/locate/compstruct

A computational multi-scale approach for the stochastic mechanical response of foam-filled honeycomb cores

E.I. Saavedra Flores [a,b,*], F.A. DiazDelaO [a], M.I. Friswell [a], J. Sienz [a]

[a] College of Engineering, Swansea University, Singleton Park, Swansea SA2 8PP, United Kingdom
[b] Departamento de Ingeniería en Obras Civiles, Universidad de Santiago de Chile, Av. Ecuador 3659, Santiago, Chile

ARTICLE INFO

Article history:
Available online 28 November 2011

Keywords:
Multi-scale analysis
Gaussian stochastic process
Uncertainty analysis
Honeycomb cores
Finite element method

ABSTRACT

This paper investigates the uncertainty in the mechanical response of foam-filled honeycomb cores by means of a computational multi-scale approach. A finite element procedure is adopted within a purely kinematical multi-scale constitutive modelling framework to determine the response of a periodic arrangement of aluminium honeycomb core filled with PVC foam. By considering uncertainty in the geometric properties of the microstructure, a significant computational cost is added to the solution of a large set of microscopic equilibrium problems. In order to tackle this high cost, we combine two strategies. Firstly, we make use of symmetry conditions present in a representative volume element of material. Secondly, we build a statistical approximation to the output of the computer model, known as a Gaussian process emulator. Following this double approach, we are able to reduce the cost of performing uncertainty analysis of the mechanical response. In particular, we are able to estimate the 5th, 50th, and 95th percentile of the mechanical response without resorting to more computationally expensive methods such as Monte Carlo simulation. We validate our results by applying a statistical adequacy test to the emulator.

1. Introduction

Over the last two decades, homogenisation-based multi-scale constitutive modelling techniques relying on the volume averaging of the stress and strain fields over a Representative Volume Element (RVE) of material have attracted considerable attention within the computational mechanics community [1–7]. The interest in this area stems mainly from the suitability of multi-scale models of this type for finite element implementation and, probably more importantly, from their potential ability to capture the non-linear response by means of conventional internal variable-based phenomenological models. Such models offer the possibility of describing more accurately the stress response under complex strain paths, although they suffer from the drawback of excessive computing costs. These costs are usually acceptable when finite element analyses of single RVEs are carried out in the context of deterministic problems (refer, for instance, to Refs. [8,4,9]). However, when parametric uncertainty is considered in the context of multi-scale problems, the computational cost of solving the computer model can quickly become prohibitive. In such cases, even with the use of simple phenomenological models and relatively coarse RVE meshes, computing costs may rise by several orders of magnitude when compared to deterministic single-scale analyses.

In recent years, a significant number of components in engineering structures incorporate honeycomb cores [10] because of their high bending stiffness, strength and light weight. Important enhancements have been made in this context by filling the honeycomb system with polymer foams [11–13]. As noted by Burlayenko and Sadowski [14], this method is inexpensive and does not add a significant amount of weight to a sandwich structure. As a result, the honeycomb microstructure with incorporated foam is more effective to withstand crash, impact and fatigue loading conditions [14]. Nevertheless, the mechanical properties of polymers show a significant variability due to porosity, microscopic cracks and inclusions. Furthermore, the honeycomb-cored material systems present considerable scatter because of manufacturing induced-defects, such as misalignment and asymmetries in the metallic components. Because of its increasing importance in engineering applications, this paper investigates the uncertainty in the mechanical response of foam-filled honeycomb cores by means of a computational multi-scale approach. In particular, we assess the impact of the uncertainty in the geometric properties of a honeycomb-cored panel on its mechanical response in three different loading directions.

In order to address the issue of the very high computational cost introduced by considering parametric uncertainty in a fully coupled multi-scale analyses, we make use of implicit symmetry conditions present in the RVE of a material. Here, staggered-translational and point symmetry [15,16] are considered at the same time, which leads to the choice of the smallest possible RVE domain. In addition,

* Corresponding author. Tel.: +44 (0)1792 205678; fax: +44 (0)1792 295157.
E-mail address: e.i.saavedra-flores@swansea.ac.uk (E.I. Saavedra Flores).

0263-8223/$ - see front matter © 2012 Published by Elsevier Ltd.
doi:10.1016/j.compstruct.2011.11.001

we employ a less expensive surrogate of a finite element model. This finite element model or code (henceforth referred to as a *simulator*) can be understood as a function $\eta : \mathbb{R}^{d_1} \rightarrow \mathbb{R}^{d_2}$ that, given an input $\mathbf{x}$, it returns an output $\mathbf{y} = \eta(\mathbf{x})$. Several strategies that reduce the computational cost of expensive simulators by approximating their output can be found in the literature [17,18]. Based on different underlying methodologies, these strategies are referred to as metamodels, response surfaces, auxiliary models, among many others [19]. A particular kind of metamodel, usually employed in the analysis and design of computer experiments [20,21], is Gaussian process emulation. This metamodel constructs a statistical approximation to the code's output, called a Gaussian process emulator (GPE). The main idea is the following: A small set of simulator runs is treated as training data used to update the prior beliefs about the output. As explained later, these prior beliefs take the form of a Gaussian stochastic process. After conditioning on the training data and updating, the mean of the resulting posterior distribution provides a fast approximation to the code's output at any untried input, whereas it returns the known value of the code at each of the initial runs. Gaussian process emulators have already been implemented in several scientific fields, such as test crash modelling [22] and structural dynamics [23,24]. Many other examples are available in the literature.

The paper is organised as follows. Section 2 presents the essential equations associated with the homogenisation problem in continuum form. Section 3 shows the finite element approximation to the generic multi-scale constitutive model of periodic media with symmetry considerations. A brief overview of Gaussian process emulation is presented in Section 4. The finite element modelling of foam-filled honeycomb cores is described in Section 5. Section 6 shows numerical results obtained from the present multi-scale and metamodelling approach. The validation of the emulator is presented in Section 7. Finally, Section 8 summarises the main conclusions of this work.

2. Homogenisation-based multi-scale constitutive theory

The main assumption in the homogenisation-based multi-scale constitutive theories of solids is that the macroscopic or homogenised strain tensor $\boldsymbol{\varepsilon}$ at any arbitrary point $\boldsymbol{x}$ of the macroscopic continuum is the volume average of the microscopic strain tensor field $\boldsymbol{\varepsilon}_\mu$ over the domain Ω_μ of the local RVE. Similarly, the macroscopic or homogenised stress tensor field $\boldsymbol{\sigma}$ is assumed to be the volume average of the microscopic stress tensor $\boldsymbol{\sigma}_\mu$, over Ω_μ. For any instant t, the above conditions can be expressed mathematically as

$$\boldsymbol{\varepsilon}(\boldsymbol{x},t) = \frac{1}{V_\mu}\int_{\Omega_\mu} \boldsymbol{\varepsilon}_\mu(\boldsymbol{y},t)dV \quad \text{and } \boldsymbol{\sigma}(\boldsymbol{x},t) = \frac{1}{V_\mu}\int_{\Omega_\mu} \boldsymbol{\sigma}_\mu(\boldsymbol{y},t)dV, \tag{1}$$

in which V_μ is the volume of the RVE associated to point $\boldsymbol{x}$, and $\boldsymbol{y}$ is the local RVE coordinates. Furthermore, the microscopic strain tensor $\boldsymbol{\varepsilon}_\mu$ can be related to the local displacement field $\boldsymbol{u}_\mu$ by means of the standard expression $\boldsymbol{\varepsilon}_\mu \equiv \nabla^s \boldsymbol{u}_\mu$, in which ∇^s is the symmetric gradient operator. In addition, it is possible to decompose the displacement field $\boldsymbol{u}_\mu$ as a sum of a linear displacement $\boldsymbol{\varepsilon}(\boldsymbol{x},t)\boldsymbol{y}$, which represents a homogeneous strain, and a displacement fluctuation field $\tilde{\boldsymbol{u}}_\mu$. The displacement fluctuations field represents local variations about the linear displacement $\boldsymbol{\varepsilon}(\boldsymbol{x},t)\boldsymbol{y}$ and do not contribute to the macroscopic scale strain.

By taking into account the Hill–Mandel Principle of Macrohomogeneity [25,26], which establishes that the macroscopic stress power must equal the volume average of the microscopic stress power over Ω_μ, the virtual work equation for the RVE can be reduced to

$$\int_{\Omega_\mu} \boldsymbol{\sigma}_\mu(\boldsymbol{y},t) : \nabla^s \boldsymbol{\eta}\, dV = 0, \tag{2}$$

with $\boldsymbol{\eta}$ representing the virtual kinematically admissible displacements field of the RVE.

In order to make problem (2) well-posed, a set of kinematical constraints upon the selected RVE is required. In what follows, the choice of this set will coincide with the widely used Periodic boundary displacement fluctuations model, which is typically associated with the modelling of periodic media. Here, the fundamental kinematical assumption consists of prescribing identical displacement fluctuation vectors for each pair of opposite points $\boldsymbol{y}_+$ and $\boldsymbol{y}_-$ on the RVE boundary $\partial\Omega_\mu$, such that:

$$\tilde{\boldsymbol{u}}_\mu(\boldsymbol{y}_+,t) = \tilde{\boldsymbol{u}}_\mu(\boldsymbol{y}_-,t). \tag{3}$$

By describing the RVE response by means of a generic local dissipative constitutive theory, the microscopic stress tensor $\boldsymbol{\sigma}_\mu$ is represented by a functional of the history of $\boldsymbol{\varepsilon}_\mu$, which is expressed symbolically as $\boldsymbol{\sigma}_\mu(\boldsymbol{y},t) = \mathfrak{F}_y\left(\boldsymbol{\varepsilon}_\mu^t(\boldsymbol{y})\right)$. The functional $\mathfrak{F}_y$ associated with point $\boldsymbol{y}$ maps the strain history, $\boldsymbol{\varepsilon}_\mu^t$, up to time t, into the stress $\boldsymbol{\sigma}_\mu$ of time t. In view of the above constitutive assumption and the additive decomposition of the microscopic displacement field, the equilibrium Eq. (2) leads to

$$G(\boldsymbol{\varepsilon},\tilde{\boldsymbol{u}}_\mu,\boldsymbol{\eta}) \equiv \int_{\Omega_\mu} \mathfrak{F}_y\{[\boldsymbol{\varepsilon}(\boldsymbol{x},\boldsymbol{t}) + \nabla^s \tilde{\boldsymbol{u}}_\mu(\boldsymbol{y},t)]^t\} : \nabla^s \boldsymbol{\eta}\, dV = 0, \tag{4}$$

where we have defined G as virtual work functional.

Definition (*Microscopic equilibrium problem*). Eq. (4) defines the *microscopic equilibrium problem* stated as follows: Given the history of the macroscopic strain tensor $\varepsilon = \varepsilon(x,t)$, at a point x of the macrocontinuum, find a kinematically admissible microscopic displacement fluctuation field $\tilde{\boldsymbol{u}}_\mu$, such that for each instant t, Eq. (4) is satisfied [27].

3. Finite element implementation

This section describes the numerical approximation of multi-scale constitutive models by means of the finite element method, when both staggered-translational and point symmetry [15,16] are taken into account. A generic non-linear implicit finite element discretisation scheme is used as the underlying framework. In what follows, the microscopic constitutive response that characterises the behaviour of the RVE material is assumed to be described within the framework of continuum thermodynamics with internal variables [28,29].

The first crucial component of the implicit finite element approximation consists of an incremental (time-discrete) counterpart of the original microscopic constitutive law. In this case, an implicit numerical algorithm is used to discretise the rate constitutive equations of the internal variable-based model. Within a time interval $\Delta t = t_{n+1} - t_n$, with a given initial value $\boldsymbol{\alpha}_n$ for the set of internal variables at time t_n, the microscopic stress tensor $\boldsymbol{\sigma}_\mu|_{n+1}$ at time t_{n+1} is determined by the chosen numerical integration algorithm as a function of the microscopic strain tensor $\boldsymbol{\varepsilon}_\mu|_{n+1}$ at time t_{n+1}. This procedure gives rise to an approximate incremental constitutive function, $\hat{\boldsymbol{\sigma}}_\mu$, for the stress tensor, such that $\boldsymbol{\sigma}_\mu|_{n+1} = \hat{\boldsymbol{\sigma}}_\mu(\boldsymbol{\varepsilon}_{n+1} + \nabla^s \tilde{\boldsymbol{u}}_\mu|_{n+1}, \Delta t; \boldsymbol{\alpha}_n)$.

The following basic ingredient in the finite element approximation to the considered multi-scale models is the incremental counterpart of the microscopic equilibrium problem (4). By replacing the time-continuum constitutive functional $\mathfrak{F}_y$ of (4) with its time-discrete counterpart, $\hat{\boldsymbol{\sigma}}_\mu$, the incremental equilibrium problem of step $n+1$ can be obtained straightforwardly. Finally, to complete the numerical approximation of the model, a standard finite element discretisation h is introduced. By replacing the domain Ω_μ with its discrete counterpart Ω_μ^h, the fully spatial-temporal discretised version of (4) is obtained:

$$G^h(\tilde{\mathbf{u}}_\mu|_{n+1}) \equiv \left\{ \int_{\Omega_\mu^h} \mathbf{B}^\top \hat{\sigma}_\mu(\boldsymbol{\varepsilon}_{n+1} + \mathbf{B}\tilde{\mathbf{u}}_\mu|_{n+1})\, dV \right\} \cdot \boldsymbol{\eta} = 0, \tag{5}$$

in which $\mathbf{B}$ denotes the global strain–displacement matrix, $\boldsymbol{\varepsilon}_{n+1}$ is the prescribed finite element array of macroscopic engineering strains at time t_{n+1}, $\hat{\boldsymbol{\sigma}}_\mu$ is the incremental constitutive functional at the RVE level that delivers the array of stress components, $\tilde{\mathbf{u}}_\mu|_{n+1}$ is the array of global nodal displacement fluctuations and $\boldsymbol{\eta}$ is the array of global nodal virtual displacements.

Within the present framework, the algebraic equation system (5) is solved by the quadratically convergent Newton–Raphson iterative procedure. Then, with a given $\boldsymbol{\varepsilon}_{n+1}$, the following equation system is solved for the iterative correction $\delta\tilde{\mathbf{u}}_\mu^{(k)}$ to the displacement fluctuation during the typical Newton iteration (k):

$$[\mathbf{F}^{(k-1)} + \mathbf{K}^{(k-1)}\delta\tilde{\mathbf{u}}_\mu^{(k)}] \cdot \boldsymbol{\eta} = 0, \tag{6}$$

where $\mathbf{F}^{(k-1)}$ is the residual vector, and $\mathbf{K}^{(k-1)}$ the tangent stiffness matrix.

For the specific purpose of this work, we exploit the existence of both staggered-translational and point symmetry conditions in a honeycomb configuration. In this context, the presence of these additional symmetries allows the choice of an RVE with domain comprising only one symmetric portion of the original domain. Whenever such conditions are met, substantial reductions in computational costs associated with CPU time and storage requirements are achieved.

In order to incorporate the above symmetry considerations in the finite element implementation of Eq. (6), we reduce the analysis of the original full RVE domain into one quarter as shown in Fig. 1, with the following subsets of nodes in the finite element mesh: one set of interior nodes, with corresponding quantities denoted by the subscript i; one set of corner nodes of the unit cell, denoted by o_1, o_2, o_3, and o_4; and two sets of boundary nodes denoted, respectively, with subscripts $\oplus$ and $\ominus$, so that for each node of set $\oplus$ with coordinate $\boldsymbol{y}_\oplus$ there is an equidistant node about the midpoint of each side with coordinate $\boldsymbol{y}_\ominus$ that belongs to the set $\ominus$ (refer to Fig. 2 for further details). The relationship between $\oplus$ and $\ominus$ is such that a one-to-one correspondence is satisfied between these two sets of nodes.

By applying this partition to the components of $\mathbf{F}, \mathbf{K}, \delta\tilde{\mathbf{u}}_\mu$ and $\boldsymbol{\eta}$, and by enforcing staggered-translational and point symmetry kinematical constraints simultaneously with Eq. (3), the Newton–Raphson Eq. (6) can be explicitly written as [15]

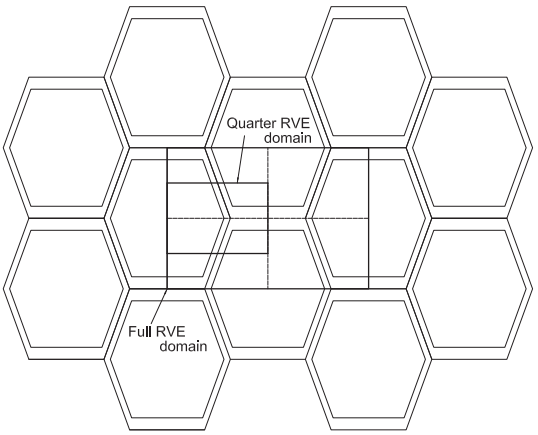

Fig. 1. Reduction of full RVE domain into one quarter.

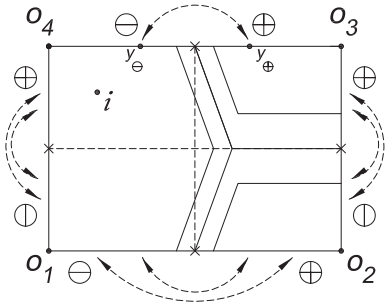

Fig. 2. Schematic diagram of the quarter RVE domain chosen for the analyses. Set of points $i, o_1 \cdots o_4, \oplus$ and $\ominus$ have been indicated here. The $\times$-symbols show the midpoint of each side of the reduced RVE domain such that equidistant points with coordinates $\boldsymbol{y}_\oplus$ and $\boldsymbol{y}_\ominus$ belonging to the sets $\oplus$ and $\ominus$, respectively, satisfy a one-to-one correspondence.

$$\begin{bmatrix} \mathbf{k}_{ii} & \mathbf{k}_{i\oplus} - \mathbf{k}_{i\ominus} & \mathbf{k}_{io_1} - \mathbf{k}_{io_2} + \mathbf{k}_{io_3} - \mathbf{k}_{io_4} \\ \mathbf{k}_{\ominus i} - \mathbf{k}_{\ominus i} & \mathbf{k}_{\ominus\oplus} - \mathbf{k}_{\ominus\ominus} - \mathbf{k}_{\ominus\oplus} + \mathbf{k}_{\ominus\ominus} & \mathbf{k}_{\ominus o_1} - \mathbf{k}_{\ominus o_2} + \mathbf{k}_{\ominus o_3} - \mathbf{k}_{\ominus o_4} - \mathbf{k}_{\ominus o_1} + \mathbf{k}_{\ominus o_2} - \mathbf{k}_{\ominus o_3} + \mathbf{k}_{\ominus o_4} \\ \mathbf{k}_{o_1 i} - \mathbf{k}_{o_2 i} + \mathbf{k}_{o_3 i} - \mathbf{k}_{o_4 i} & \mathbf{k}_{o_1\oplus} - \mathbf{k}_{o_1\ominus} - \mathbf{k}_{o_2\oplus} + \mathbf{k}_{o_2\ominus} + \mathbf{k}_{o_3\oplus} - \mathbf{k}_{o_3\ominus} - \mathbf{k}_{o_4\oplus} + \mathbf{k}_{o_4\ominus} & \mathbf{k}_I - \mathbf{k}_{II} + \mathbf{k}_{III} - \mathbf{k}_{IV} \end{bmatrix}^{(k-1)} \begin{bmatrix} \delta\tilde{\mathbf{u}}_i \\ \delta\tilde{\mathbf{u}}_\oplus \\ \delta\tilde{\mathbf{u}}_{o_1} \end{bmatrix}^{(k)} = - \begin{bmatrix} \mathbf{F}_i \\ \mathbf{F}_\oplus - \mathbf{F}_\ominus \\ \mathbf{F}_{o_1} - \mathbf{F}_{o_2} + \mathbf{F}_{o_3} - \mathbf{F}_{o_4} \end{bmatrix}^{(k-1)}, \tag{7}$$

with

$$\mathbf{k}_I = \mathbf{k}_{o_1o_1} - \mathbf{k}_{o_1o_2} + \mathbf{k}_{o_1o_3} - \mathbf{k}_{o_1o_4}, \quad \mathbf{k}_{II} = \mathbf{k}_{o_2o_1} - \mathbf{k}_{o_2o_2} + \mathbf{k}_{o_2o_3} - \mathbf{k}_{o_2o_4},$$
$$\mathbf{k}_{III} = \mathbf{k}_{o_3o_1} - \mathbf{k}_{o_3o_2} + \mathbf{k}_{o_3o_3} - \mathbf{k}_{o_3o_4}, \quad \mathbf{k}_{IV} = \mathbf{k}_{o_4o_1} - \mathbf{k}_{o_4o_2} + \mathbf{k}_{o_4o_3} - \mathbf{k}_{o_4o_4}.$$

4. Metamodelling

4.1. Gaussian process emulation

Let $\eta(\cdot)$ be an expensive code, such that the associated computational cost makes it affordable to evaluate it only at a limited number of points in the input domain. This uncertainty about the output of $\eta(\cdot)$ can be modelled through a probability distribution [30]. Following a Bayesian treatment [31], the prior beliefs about the relationship between the input and the unknown output are conditioned on a set of evaluations of $\eta(\cdot)$, therefore combining subjective and objective information. Assume that $\eta(\cdot)$ can be represented by

$$\eta(\cdot) = \mathbf{h}(\cdot)^\top \boldsymbol{\beta} + Z(\cdot) \tag{8}$$

where $\mathbf{h}(\cdot)$ is a vector of known functions and $\boldsymbol{\beta}$ is a vector of unknown coefficients. The vector $\mathbf{h}(\cdot)$ should be chosen to reflect the available information about the functional form of $\eta(\cdot)$ [32,33]. The function $Z(\cdot)$ is a stochastic process with mean zero and covariance function $Cov(\cdot, \cdot)$. Let $\mathbf{y} = [\eta(\mathbf{x_1}), \ldots, \eta(\mathbf{x_n})]^\top$ be a vector of observations corresponding to the inputs $\mathbf{x_1}, \ldots, \mathbf{x_n}$. These observations are used to update the prior distribution of $\eta(\cdot)$. An analytically convenient choice for such prior is the following Gaussian process distribution [34]

$$\eta(\cdot)|\boldsymbol{\beta}, \sigma^2 \sim \mathcal{N}(\mathbf{h}(\cdot)^\top \boldsymbol{\beta}, \sigma^2 C(\cdot, \cdot)) \tag{9}$$

where $\mathbf{h}(\cdot)$ and $\boldsymbol{\beta}$ are defined as above. The covariance function consists of a variance σ^2 and a correlation function $C(\cdot, \cdot)$.

Definition (*Gaussian stochastic process*). Let $\mathbf{x} \in \mathbb{R}^N$. $Z(\cdot)$ is a Gaussian stochastic process if for any $n \geqslant 1$ and any choice $\{\mathbf{x_1}, \ldots, \mathbf{x_n}\}$, the vector $[Z(\mathbf{x_1}), \ldots, Z(\mathbf{x_n})]^\top$ has a multivariate normal distribution.

In order to choose a valid correlation function $C(\cdot,\cdot)$, some authors [21] consider correlation functions that are products of one dimensional correlations, specifically functions of the form

$$C(\mathbf{x}, \mathbf{x}') = \prod_{i=1}^{n} \exp\left\{-b_i |\mathbf{x_i} - \mathbf{x_i'}|^{\alpha}\right\} \tag{10}$$

where $b_i > 0$ for all i, and where $\alpha > 0$. In particular, if $\alpha = 2$, then $C(\cdot,\cdot)$ is infinitely differentiable. This feature is convenient when Gaussian processes are used to model not only the code output $\eta(\cdot)$, but also its derivatives [35]. For these reasons, a popular choice of correlation function is

$$C(\mathbf{x}, \mathbf{x}') = \exp\left\{-(\mathbf{x} - \mathbf{x}')^\top \mathbf{B} (\mathbf{x} - \mathbf{x}')\right\} \tag{11}$$

where $\mathbf{B}$ is a diagonal positive definite matrix. The diagonal of $\mathbf{B}$ is a vector $\mathbf{b} \in \mathbb{R}_+^n$ of smoothness parameters. These parameters quantify the rate at which the output varies as any $\mathbf{x}$ varies. One available technique [36] to estimate these parameters is to derive the density function $f(\mathbf{B}|\mathbf{y})$ and obtain a maximum likelihood estimator of $\mathbf{b}$.

After conditioning on the training runs $(\mathbf{x_1}, \eta(\mathbf{x_1})), \ldots, (\mathbf{x_n}, \eta(\mathbf{x_n}))$ and updating the prior distribution (9), the mean of the resulting posterior distribution approximates the output of $\eta(\cdot)$ at any untried $\mathbf{x}$, whereas it reproduces the known output at each one of the inputs $\mathbf{x_1}, \ldots, \mathbf{x_n}$. The variance of the posterior distribution quantifies the uncertainty that arises from having only a limited number of evaluations of $\eta(\cdot)$ [37]. Very conveniently, the posterior is also a Gaussian process distribution of the form

$$\eta(\cdot)|\mathbf{y}, \sigma^2 \sim \mathcal{N}(m^{**}(\cdot), \sigma^2 C^{**}(\cdot,\cdot)) \tag{12}$$

Since it can be shown that $m^{**}(\cdot)$ does not include any term involving the expensive code $\eta(\cdot)$, it is a fast approximation of $\eta(\mathbf{x})$ for any $\mathbf{x}$ in its domain. The conditioning on σ^2 can also be eliminated, such that

$$\frac{\eta(\mathbf{x}) - m^{**}(\mathbf{x})}{\hat{\sigma}\sqrt{\frac{(n-q-2)C^{**}(\mathbf{x})}{n-q}}} \sim t_{n-q} \tag{13}$$

which is a Student's t-distribution with $n - q$ degrees of freedom (not to be confused with the degrees of freedom in a finite element method context). The complete process is summarised in Algorithm 1. The expressions defined above, such as $m^{**}(\cdot)$ and $C(\cdot,\cdot)^{**}$, are defined in the Appendix.

Algorithm 1. Gaussian process emulation

Input: Design points $\{\mathbf{x_i}\}_{i=1}^n$
Output: Predictive mean $\mathbf{E}[\eta(\mathbf{x})|\mathbf{y}] = m^{**}(\mathbf{x})$ and variance $\mathbf{Var}[\eta(\mathbf{x})|\mathbf{y}] = \sigma^2 C^{**}(\cdot,\cdot)$
begin
1. Select n design points $\{\mathbf{x_i}\}_{i=1}^n$
2. Obtain the vector of observations $\mathbf{y} = [\eta(\mathbf{x_1}), \ldots, \eta(\mathbf{x_n})]^\top$
3. Update the prior distribution (9) using $\mathbf{y}$ and obtain the posterior distribution (12)
4. Compute the predictive mean $m^{**}(\mathbf{x})$ and variance $\sigma^2 C^{**}(\cdot,\cdot)$ for any untried $\mathbf{x}$
end

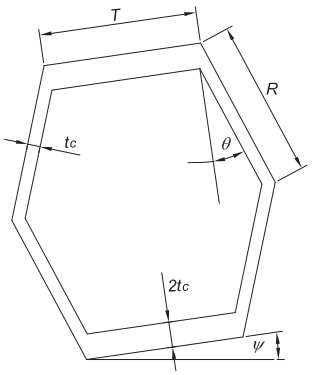

Fig. 3. Geometric parameters which define the honeycomb microstructure.

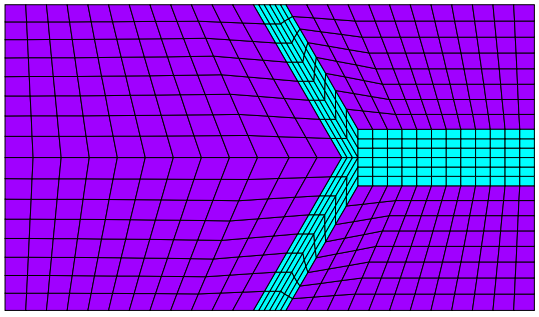

Fig. 4. Typical microscopic finite element mesh adopted for the computational homogenisation of the periodic microstructure.

4.2. Uncertainty Analysis using GPEs

Being the implementation of a computer code, a simulator $\eta(\cdot)$ is deterministic. This means that if it is run repeatedly at the same input $\mathbf{x}$, it will always return the same output $\mathbf{y} = \eta(\mathbf{x})$. However, the inputs we are interested in are physical constants, the values of which are unknown. In the probabilistic uncertainty analysis of deterministic simulators, the values of the uncertain inputs are considered to be a random variable $\mathbf{X}$. Thus, the output of the simulator is also a random variable, denoted by $\mathbf{Y} = \eta(\mathbf{X})$. To begin the uncertainty analysis, the first stage is to quantify the uncertainty in $\mathbf{X}$ by specifying a probability distribution $\mathcal{F}(\mathbf{X})$. The aim of uncertainty analysis is to propagate the uncertainty in $\mathbf{X}$ through the simulator $\eta(\cdot)$ in order to characterise the distribution of $\mathbf{Y}$. If $\eta(\cdot)$ were not an expensive simulator, the most straightforward uncertainty analysis would proceed by drawing a large sample $\{\mathbf{x_1}, \ldots, \mathbf{x_N}\}$ from the input distribution $\mathcal{F}(\mathbf{X})$ and then running the simulator at each of them. This would result in a sample of outputs $\{\mathbf{y_1}, \ldots, \mathbf{y_N}\}$ from which any statistic or summary $\mathcal{S}(\mathbf{Y})$ can be estimated. $\mathcal{S}(\mathbf{Y})$ could be the mean, the variance, a particular quantile, or any other summary.

A straightforward way to use a GPE to carry out uncertainty analysis would be to substitute $\eta(\cdot)$ with the predictive mean $m^{**}(\mathbf{x})$. Potentially, this predictive mean can be evaluated a large number of times at any untried input at very low cost, alleviating the computational burden of the expensive simulator. However, this basic Monte Carlo approach does not incorporate the fact that any summary $\mathcal{S}(\mathbf{Y})$ is a function of an unknown quantity and thus is itself uncertain. The solution to this is detailed in Algorithm 2, which is a modified Monte Carlo algorithm proposed in [38] that incorporates the uncertainty inherent to $\mathcal{S}(\mathbf{Y})$ into the analysis.

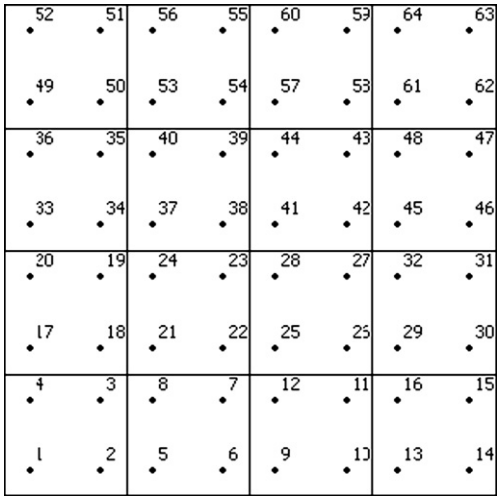

Fig. 5. Typical macroscopic finite element mesh used in the modelling of the foam-filled honeycomb-cored panel under in-plane loading conditions. Gauss quadrature points are also shown here.

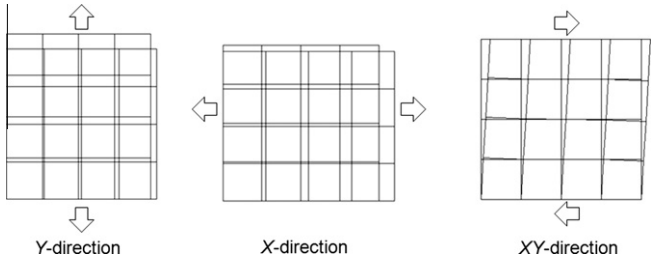

Fig. 6. Loading programmes adopted for the analysis of the mechanical response of the honeycomb-cored panel under in-plane loading conditions.

Algorithm 2. Uncertainty analysis using a GPE.

Input: Sample $\{\mathbf{x_i}\}_{i=1}^{N}$ from the input distribution $\mathcal{F}(\mathbf{X})$
Output: Summary $\mathcal{S}(\mathbf{Y})$ of the output distribution $\mathbf{Y}$
begin
1. Draw a sample $\{\mathbf{x_i}\}_{i=1}^{N}$ from the distribution $\mathcal{F}(\mathbf{X})$
2. Draw a random function $\eta_{(j)}$ from the emulator posterior distribution (12)
3. Evaluate $\eta_{(j)}(\mathbf{x_1}), \ldots, \eta_{(j)}(\mathbf{x_N})$
4. Obtain $\mathcal{S}_j(\mathbf{Y})$, the Monte Carlo estimate of $\mathcal{S}(\mathbf{Y})$
5. Repeat steps 1–3 and obtain the sample $\mathscr{S} = \{\mathcal{S}_1(\mathbf{Y}), \ldots, \mathcal{S}_{N_\eta}(\mathbf{Y})\}$
6. Use $\mathscr{S}$ to estimate any summary of the distribution of $\mathcal{S}(\mathbf{Y})$
end

5. Finite element modelling of foam-filled honeycomb cores

In this section, we consider the fully coupled two-scale finite element modelling of a honeycomb-cored panel under in-plane loading conditions. The particular honeycomb microstructure has been obtained from Burlayenko and Sadowski [14]. It consists of a periodic arrangement of aluminium hexagonal honeycomb core filled with polyvinyl chloride (PVC) foam. The geometric parameters which define the periodic microstructure are the angle θ, the in-plane rotation ψ, the thickness t_c and the lengths T and R (refer to Fig. 3). In this study, the corresponding baseline values are taken as: $R = 1$ mm, $T = 1$ mm, $tc = 0.08$ mm, $\theta = 30°$ and $\psi = 0°$.

The materials are modelled here by an elastic-perfectly plastic von Mises law. The corresponding mechanical properties for aluminium are: Young modulus $E = 72$ GPa, Poisson ratio $v = 0.31$ and yield stress $\sigma_y = 405$ MPa [14]. For the PVC filler, we adopt a Young modulus $E = 0.23$ GPa, Poisson ratio $v = 0.32$ and yield stress

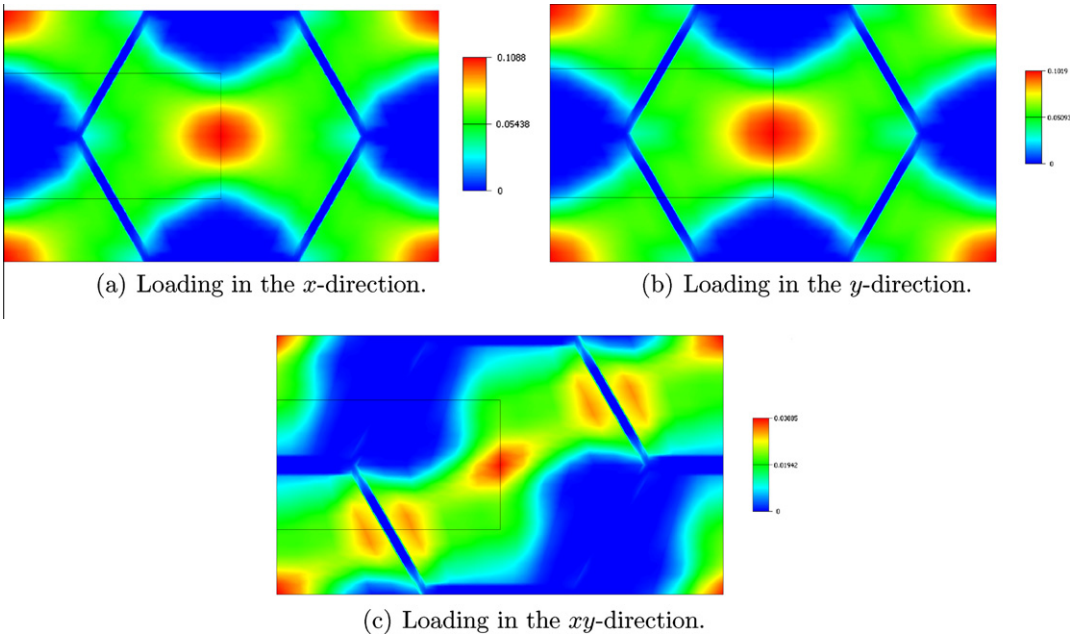

Fig. 7. Contour diagrams for the equivalent plastic strains in the RVE located at Gauss-point 1 of the macroscopic mesh, at the final stage of the loading programme. For the sake of clarity, the contour plot in the quarter RVE domain (enclosed by a black square) is shown for each direction with its repetition (four times) in the full RVE domain (when no symmetry conditions are taken into account).

σ_y = 5.75 MPa [14]. For all of the finite element analyses we assume plane strain conditions under an infinitesimal strains regime.

To eliminate volumetric locking, the F-Bar methodology [39] is adopted throughout. A typical RVE finite element mesh is shown in Fig. 4. It contains 552 F-bar four-noded quadrilateral elements with a total number of 606 nodes.

The computational effort required for the solution of the (microscopic) RVE equilibrium problem is directly related to the number of degrees of freedom of the discretised RVE domain. As explained in Section 3, the presence of both staggered-translational and point symmetry conditions allows the choice of an RVE domain comprising only one quarter of the original domain, in which substantial savings in terms of computing times and memory requirements are achieved.

The macroscopic problem consists of a 40 × 40 cm panel whose material law is defined by the computational homogenisation of the above honeycomb microstructure. A mesh of 16 F-bar fournoded quadrilateral elements with a total of 25 nodes is used to discretise one symmetric portion of the problem domain with appropriate boundary constraints imposed along the symmetry lines. The macroscopic finite element mesh is shown in Fig. 5.

The loading programme consists of applying a prescribed displacement of 2 cm in three different directions as shown in Fig. 6. In all of the cases, *x* and *y*-axes coincide respectively with the hor-

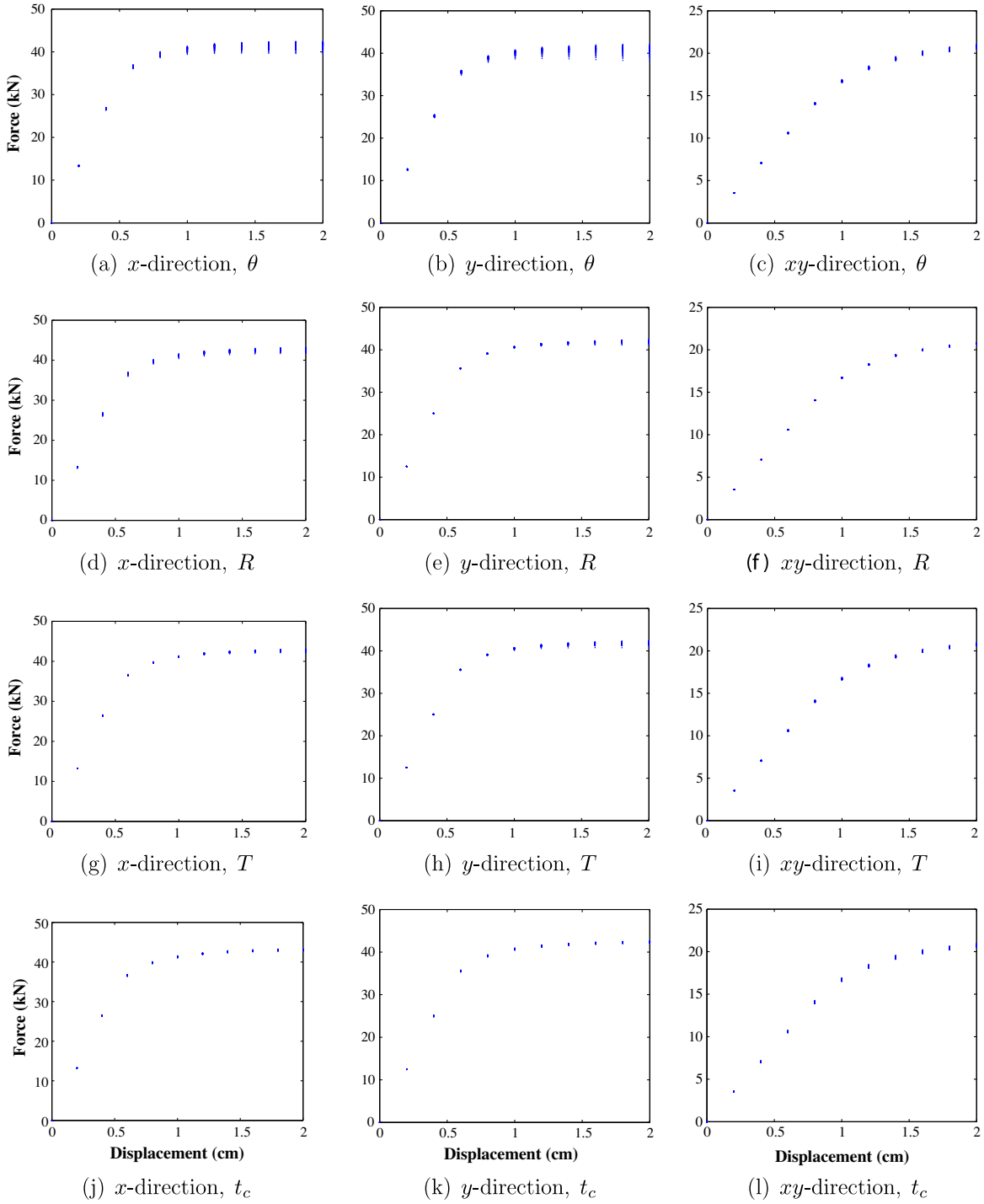

Fig. 8. Force–displacement curves when parameters θ, R, T and t_c are perturbed in turn, for each loading direction.

izontal and vertical directions. The *xy*-direction is associated with in-plane shear deformation of the panel. The total prescribed displacement is applied in each direction of analysis in 10 incremental steps. However, when no convergence is detected in the solution of the RVE equilibrium problem at any macroscopic Gauss point, smaller load increments are taken into account to ensure the success of the whole macroscopic loading programme. We remark that during each load step of the fully coupled two-scale analysis the macroscopic equilibrium problem is solved simultaneously with 64 RVE equilibrium problems at the macroscopic Gauss-point level (refer to Fig. 5 to see the macroscopic Gauss-points).

In order to introduce uncertainty in the material definition of the above panel, we propose a modelling strategy which perturbs each of the geometric parameters shown in Fig. 3. As we are interested in understanding the influence of each of these parameters on the overall mechanical response of the panel, for each analysis, a single parameter is perturbed in turn, about its baseline value at each (macroscopic) Gauss-point of the macroscopic finite element mesh. The procedure is repeated again, for a second parameter in each direction of analysis, and so on.

6. Numerical results

As commented in the previous section, a study of the influence of random geometric parameters on the mechanical response of the homogenised material is carried out. The numerical results shown here are the effect of the incidence of the angle θ, the in-plane rotation ψ, the thickness t_c and the lengths T and R, on the force–displacement curves of the honeycomb-cored panel considered in this work for the three loading directions (refer to Fig. 6).

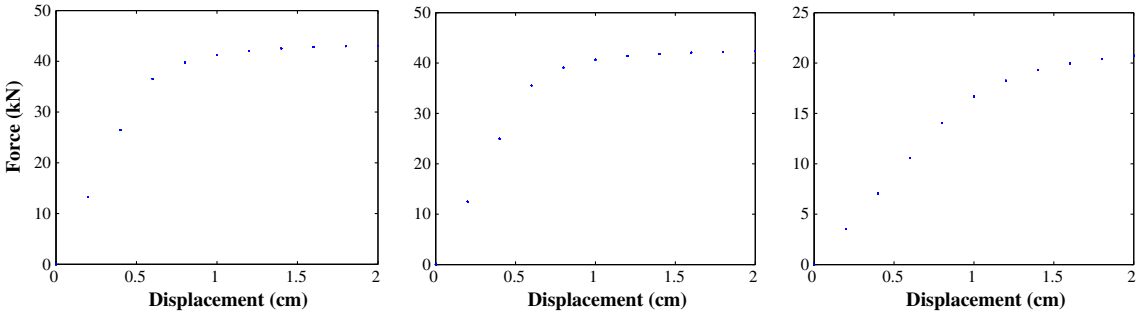

(a) x-direction, ψ (b) y-direction, ψ (c) xy-direction, ψ

Fig. 9. Force–displacement curves when parameter ψ is perturbed in each loading direction.

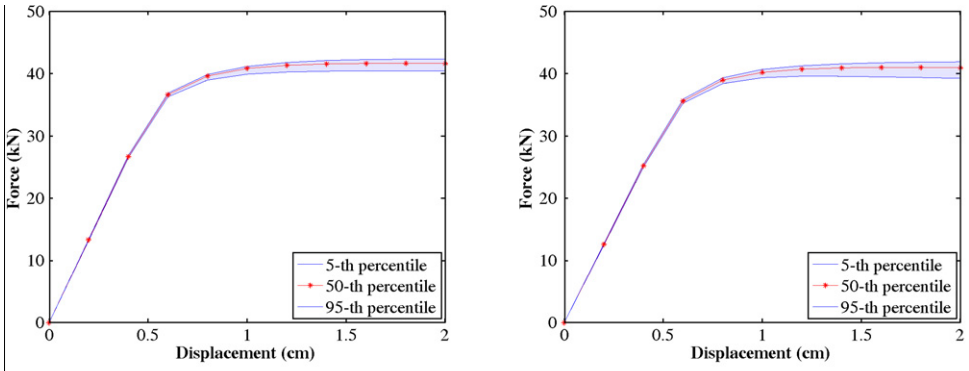

(a) Force-displacement curve in the x-direction. (b) Force-displacement curve in the y-direction.

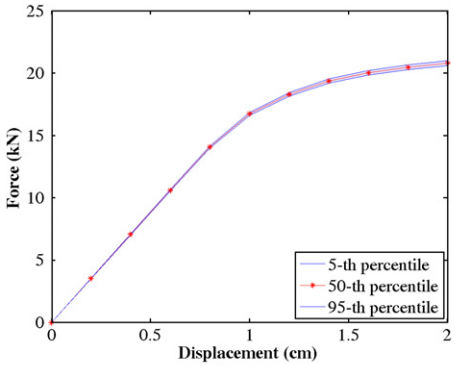

(c) Force-displacement curve in the xy-direction.

Fig. 10. Force-displacement curves with random angle θ, such that $\theta \sim \mathcal{N}(30, 1)$. The emulated 5th and 95th percentiles are shown in the lower and upper solid lines, respectively. The median is shown as a solid dotted line.

The forces are determined from the sum of nodal reactions along the loading directions. In particular, we are interested in the probabilistic characterisation of the mechanical response for a range of prescribed displacements up to 2 cm.

In order to gain insight into the microscopic deformation mechanisms, Fig. 7 shows some typical results obtained in our multi-scale analyses when the baseline values of R, T, tc, ψ and θ are considered in the definition of the microstructure. The contour plot of the equivalent plastic strains are shown here, in the RVE located at Gauss-point 1 of the macroscopic mesh (refer to Fig. 5), in the three loading directions, at the final stage of the loading programme. For the sake of clarity, we show our results obtained for the quarter RVE domain (enclosed by a black square) and its repetition (four times) in the full RVE domain (when no symmetry conditions are taken into account). We remark however that, all our finite element calculations considered one quarter RVE domains. For the three loading directions shown in the above figure, it is possible to observe a large accumulation of plastic strains localised in the PVC filler, particularly in the centres of each hexagon. An interesting phenomenon is also observed in Fig. 7c, in which a large amount of plastic dissipation is also concentrated in the region next to the aluminium-PVC contact, revealing potential problems of debonding during shear deformation.

As explained in the previous section, the numerical simulations are performed by perturbing each of the geometric parameters. The assumed input distribution for each length (R, T, and tc) was chosen to be Gaussian with a mean equal to the baseline value and with a variance such that 5% of the baseline value equals 3 standard deviations. Consequently, for each Gauss-point, $R \sim \mathcal{N}(1,(0.05/3)^2)$, $T \sim \mathcal{N}(1,(0.05/3)^2)$, $tc \sim \mathcal{N}(0.08,(0.05*0.08/3)^2)$. For the case of the angles we considered a standard deviation of 1°. Thus, $\theta \sim \mathcal{N}(30,1)$, $\psi \sim \mathcal{N}(0,1)$.

The statistics we are interested in determining are the 5th, 50th and 95th percentiles of the force for each displacement level (assumed to be from 0 to 2 cm with a 0.2 cm increment). As mentioned before, if it were not expensive to generate every force–displacement curve for a given value of a random parameter, say θ, then it would suffice to run a Monte Carlo analysis for a large number of realisations of θ, and the statistics of the mechanical response could be approximated to an arbitrary degree of accuracy. Since this is not the case, a small number of realisations of the force–displacement curve must be performed for a perturbation of each parameter in turn. Figs. 8 and 9 show the numerical results of these few realisations in each direction.

After an inspection of the numerical results, it is possible to observe that the parameters ψ, t_c, T and R have very little influence on the overall mechanical response of the panel, due to the proximity of the curves in each graph. However, a greater influence of the angle θ on the response of the panel is observed, particularly in the x and y-loading directions.

Since the four parameters ψ, t_c, T and R have virtually no influence on the mechanical response, we take into consideration only the parameter θ in all of our uncertainty analyses. Here, the small set of realisations of the parameter θ is taken as the inputs upon which a GPE is built. In order to infer the percentiles, we use the estimation algorithm proposed in [33], which combines the implementations of Algorithms 1 and 2. For this particular parameter, the emulated percentiles of the force–displacement curves are shown in Fig. 10, for each loading direction.

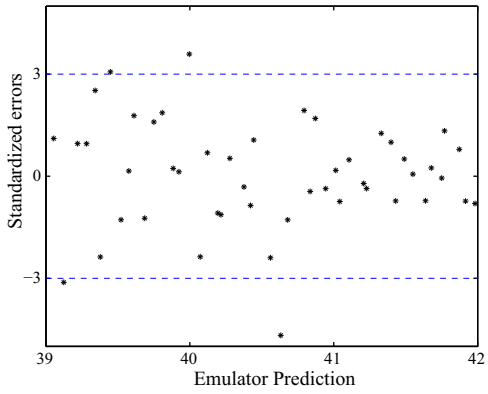

(a) Validation in the x-direction.

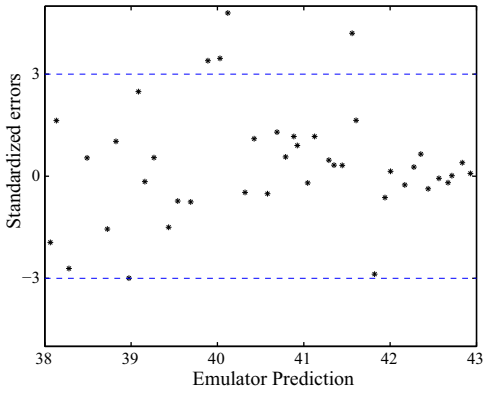

(b) Validation in the y-direction.

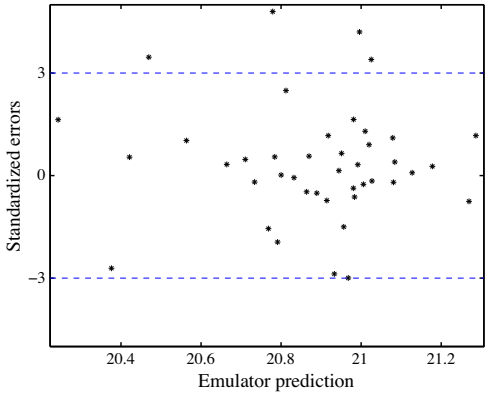

(c) Validation in the xy-direction.

Fig. 11. Individual standardised prediction errors in the three directions. The quantity of data in the interval $[-3,3]$ gives indication of the adequacy of the emulator.

For the x and y-directions, we can observe a similar degree of sensitivity of the mechanical response to changes in the angle θ. However, during the particular mechanism of shear deformation, the estimated mechanical response shows no significant sensitivity to changes in this parameter due to the proximity of the lower and upper curves associated to the 5th and 95th percentiles of the force, respectively.

7. Validation of the metamodel

Although the Gaussian process is a flexible class of distributions to represent prior beliefs about a computer model, a GPE might poorly represent the simulator due to a variety of reasons such as a wrong choice of the mean and covariance structures or a wrong choice of the training set that might induce an inappropriate estimation of parameters. To cope with these disadvantages, several methods for the validation of emulators have been proposed. In this paper, we applied the standardised prediction error method proposed in [40]. The method is detailed below.

Let $\Theta^* = \{\theta_1^*, \ldots, \theta_v^*\}$ be a set of validation points in the input domain, different from the already chosen realisations of the random parameter in turn. The corresponding validation data are $\mathbf{y}^* = [\eta(\theta_1^*), \ldots, \eta(\theta_v^*)]^\top$. A possible diagnostic of $\mathbf{y}^*$ is to calculate the standardised prediction errors of the simulator's output and the predictive mean of the emulator given the training data. That is, for $j = 1, \ldots, v$

$$\delta_j^{se}(\mathbf{y}^*) = \frac{\mathbf{y}_j^* - m^{**}\left(\eta\left(\theta_j^*\right)\right)}{\hat{\sigma}\sqrt{C^{**}\left(\eta\left(\theta_j^*\right), \eta\left(\theta_j^*\right)\right)}} \tag{14}$$

Each one of these standardised prediction errors has a Student's t-distribution, conditional on original vector of observations $\mathbf{y}$ (and on the smoothness parameters). Note that the size of the training data can be large enough such that $\delta_j^{se}(\mathbf{y}^*)$ approximates a standard normal distribution. Therefore, $\left|\delta_j^{se}(\mathbf{y}^*)\right| > 3$ for a high j would suggest the inadequacy of the Gaussian process emulator in a neighbourhood of θ_j^*.

The emulation was validated using this measure. Fig. 11 shows the predictive mean of the emulator against the standardised errors for the 50th percentile in each one of the directions, for a displacement value of 2 cm (since the largest uncertainty was observed at this level). This graph is useful to identify problems in the specification of the predictive mean, a situation that would be evident if, for example, most of the points lie in the positive area or viceversa.

8. Conclusions

This paper investigated the uncertainty in the mechanical response of foam-filled honeycomb cores by means of a finite element-based multi-scale framework. A periodic arrangement of aluminium honeycomb core filled with polyvinyl chloride (PVC) foam was chosen to study its stochastic mechanical properties and the corresponding uncertainty analyses were carried out through a metamodelling approach. Rather than carrying out a full Monte Carlo analysis, which could easily become unaffordable, GPEs were used to estimate the percentiles of the probability distribution of the load induced by random geometric properties in the microstructure. For some prescribed displacements, a reduced number of realisations of the angle θ was taken as the inputs upon which the GPEs were built. The advantage of this strategy was demonstrated by exploiting the implicit symmetry conditions existing in the RVE, along with the adoption of the metamodelling approach. That way, we were able to carry out fully coupled multi-scale analyses which would otherwise have been very computationally expensive. Finally, the validation of the GPE reveals the potential applications of the present methodology to the study of several engineering materials. This will be the subject of a future publication.

Acknowledgments

E.I. Saavedra Flores gratefully acknowledges the support of the Department of Civil Engineering, University of Santiago, Chile. E.I. Saavedra Flores and M.I. Friswell also acknowledge the support of the European Research Council through project 247045 entitled "Optimisation of Multiscale Structures with Applications to Morphing Aircraft".

Appendix A. Prior to posterior analysis

The following is an outline of the prior-to-posterior analysis discussed in Section 4. Full details can be found in the literature [33,34,41]. Suppose that the code's output $\eta(\mathbf{x})$ at an untried input $\mathbf{x}$ is to be estimated. Let $\mathbf{y} = [\eta(\mathbf{x_1}), \ldots, \eta(\mathbf{x}_n)]^\top$ be a vector of observations. Let $\mathbf{H} = [\mathbf{h}(\mathbf{x_1}), \ldots, \mathbf{h}(\mathbf{x}_n)]^\top$, and $\mathbf{A} \in \mathbb{R}^{n\times n}$ such that $\mathbf{A_{ij}} = C(\mathbf{x_i}, \mathbf{x_j}) \forall i, j \in \{1, \ldots, n\}$. Then

$$\mathbf{y}|\boldsymbol{\beta}, \sigma^2 \sim \mathcal{N}(\mathbf{H}\boldsymbol{\beta}, \sigma^2\mathbf{A}) \tag{15}$$

To incorporate the information $\mathbf{y}$ and obtain the distribution of $\eta(\cdot)$—$\mathbf{y}$, use the following result [42].

Theorem 1. *Let $\mathbf{z} \in \mathbb{R}^N$ be a random vector such that $\mathbf{z} \sim \mathcal{N}(\boldsymbol{\mu}, \boldsymbol{\Sigma})$. Partition $\mathbf{z}$ as $(\mathbf{z_1}, \mathbf{z_2})^\top$, where $\mathbf{z_1} \in \mathbb{R}^{N-n}$ and $\mathbf{z_2} \in \mathbb{R}^n$. Consequently, partition $\boldsymbol{\mu} = (\boldsymbol{\mu_1}, \boldsymbol{\mu_2})^\top$ and $\boldsymbol{\Sigma} = \begin{pmatrix} \boldsymbol{\Sigma_{11}} & \boldsymbol{\Sigma_{12}} \\ \boldsymbol{\Sigma_{21}} & \boldsymbol{\Sigma_{22}} \end{pmatrix}$, so that $\mathbf{E}[\mathbf{z_j}] = \mu_j$ and $Cov(\mathbf{z_j}, \mathbf{z_k}) = \boldsymbol{\Sigma_{jk}}$. Then, $\mathbf{z_1}|\mathbf{z_2} \sim \mathcal{N}(\tilde{\boldsymbol{\mu}}, \tilde{\Sigma})$, where $\tilde{\boldsymbol{\mu}} = \boldsymbol{\mu_1} + \boldsymbol{\Sigma_{12}}\boldsymbol{\Sigma_{22}^{-1}}(\mathbf{z_2} - \boldsymbol{\mu_2})$ and $\tilde{\boldsymbol{\Sigma}} = \boldsymbol{\Sigma_{11}} - \boldsymbol{\Sigma_{12}}\boldsymbol{\Sigma_{22}^{-1}}\boldsymbol{\Sigma_{21}}$.*

It follows that

$$\eta(\cdot)|\mathbf{y}, \boldsymbol{\beta}, \sigma^2 \sim \mathcal{N}(m^*(\cdot), \sigma^2 C^*(\cdot, \cdot)) \tag{16}$$

where

$$m^*(x) = \mathbf{h}(x)^\top\boldsymbol{\beta} + \mathbf{t}(x)\mathbf{A}^{-1}(\mathbf{y} - \mathbf{H}\boldsymbol{\beta}) \tag{17}$$

$$C^*(\mathbf{x}, \mathbf{x}') = C(\mathbf{x}, \mathbf{x}') - \mathbf{t}(\mathbf{x})^\top A^{-1}\mathbf{t}(\mathbf{x}') \tag{18}$$

$$\mathbf{t}(\mathbf{x}) = [C(\mathbf{x}, \mathbf{x_1}), \ldots, C(\mathbf{x}, \mathbf{x}_n)]^\top \tag{19}$$

Removing the conditioning on β using standard integration techniques [34], obtain the posterior distribution

$$\eta(\cdot)|\mathbf{y}, \sigma^2 \sim \mathcal{N}(m^{**}(\cdot), \sigma^2 C^{**}(\cdot, \cdot)) \tag{20}$$

where

$$m^{**}(\mathbf{x}) = \mathbf{h}(\mathbf{x})^\top\hat{\boldsymbol{\beta}} + \mathbf{t}(\mathbf{x})\mathbf{A}^{-1}(\mathbf{y} - \mathbf{H}\hat{\boldsymbol{\beta}}) \tag{21}$$

$$C^{**}(\mathbf{x}, \mathbf{x}') = C^*(\mathbf{x}, \mathbf{x}') + (\mathbf{h}(\mathbf{x})^\top - \mathbf{t}(\mathbf{x})^\top\mathbf{A}^{-1}\mathbf{H}) \times (\mathbf{H}^\top\mathbf{A}^{-1}\mathbf{H})^{-1}(\mathbf{h}(\mathbf{x}')^\top - \mathbf{t}(\mathbf{x}')^\top\mathbf{A}^{-1}\mathbf{H})^\top \tag{22}$$

$$\hat{\boldsymbol{\beta}} = (\mathbf{H}^\top\mathbf{A}^{-1}\mathbf{H})^{-1}\mathbf{H}^\top\mathbf{A}^{-1}\mathbf{y} \tag{23}$$

To estimate σ in Eq. (12), let q be the rank of $\mathbf{H}$. Then

$$\hat{\sigma}^2 = \frac{\mathbf{y}^\top(\mathbf{A}^{-1} - \mathbf{A}^{-1}\mathbf{H}(\mathbf{H}^\top\mathbf{A}^{-1}\mathbf{H})\mathbf{H}^\top\mathbf{A}^{-1})\mathbf{y}}{n - q - 2} \tag{24}$$

Gaussian process emulation consists of updating the prior distribution (9), which contains subjective information, by adding the objective

information **y**, *in order to obtain the posterior distribution (12). This enables the calculation of the predictive mean* $m^{**}(\cdot)$ *given the data* **y**.

References

[1] Michel JC, Moulinec H, Suquet P. Effective properties of composite materials with periodic microstructure: a computational approach. Comput Methods Appl Mech Eng 1999;172:109–43.

[2] Miehe C, Shotte J, Lambrecht M. Homogenization of inelastic solid materials at finite strains based on incremental minimization principles. Application to the texture analysis of polycrystals. J Mech Phys Solids 2002;50(10): 2123–67.

[3] Matsui K, Terada K, Yuge K. Two-scale finite element analysis of heterogeneous solids with periodic microstructures. Comput Struct 2004;82:593–606.

[4] Pellegrino C, Galvanetto U, Schrefler BA. Numerical homogenization of periodic composite materials with non-linear material components. Int J Numer Methods Eng 1999;46:1609–37.

[5] Castaneda PP. The effective mechanical properties of nonlinear isotropic composites. J Mech Phys Solids 1991;39:45–71.

[6] Suquet P. Overall potentials and extremal surfaces of power law or ideally plastic materials. J Mech Phys Solids 1993;41:981–1002.

[7] Terada K, Saiki I, Matsui K, Yamakawa Y. Two-scale kinematics and linearization for simultaneous two-scale analysis of periodic heterogeneous solids at finite strains. Comput Methods Appl Mech Eng 2003;192: 3531–63.

[8] Giusti SM, Blanco PJ, de Souza Neto EA, Feijóo RA. An assessment of the Gurson yield criterion by a computational multi-scale approach. Eng Comput 2009;26(3):281–301.

[9] Speirs DCD, de Souza Neto EA, Perić D. An approach to the mechanical constitutive modelling of arterial tissue based on homogenization and optimization. J Biomech 2008;41:2673–80.

[10] Bezazi A, Remillat C, Innocenti P, Scarpa F. In-plane mechanical and thermal conductivity properties of a rectangular-hexagonal honeycomb structure. Compos Struct 2008;84:248–55.

[11] Wu CL, Week CA, Sun CT. Improving honeycomb core sandwich structures for impact resistance. J Adv Mater 1995:41–7.

[12] Vaidya UK, Kamath M/V, Mahfuz H, Jeelani S. Low velocity impact response of resin infusion molded foam filled honeycomb sandwich composites. J Reinf Plastic Compos 1998;17(9):819–49.

[13] Vaziri A, Xue Z, Hutchinson JW. Metal sandwich plates with polymer foam-filled cores. J Mech Mater Struct 2006;1(1):95–125.

[14] Burlayenko VN, Sadowski T. Effective elastic properties of foam-filled honeycomb cores of sandwich panels. Compos Struct 2010;92:2890–900.

[15] Saavedra Flores EI, de Souza Neto EA. Remarks on symmetry conditions in computational homogenisation problems. Eng Comput 2010;27(4):551–75.

[16] Ohno N, Matsuda T, Wu X. A homogenization theory for elastic–viscoplastic composites with point symmetry of internal distributions. Int J Solids Struct 2001;38:2867–78.

[17] Zhou Z, Ong Y, Nair P, Keane A, Lum K. Combining global and local surrogate models to accelerate evolutionary optimization. IEEE Trans Syst Man Cybern, Part C 2006;36(6):814–23.

[18] Forrester AIJ, Sóbester A, Keane AJ. Engineering design via surrogate modelling. A practical guide. Chichester, UK: J. Wiley and Sons; 2008.

[19] Kleijnen JPC. Kriging metamodeling in simulation: a review. Eur J Oper Res 2009;192(3):707–16.

[20] Santner T, Williams B, Notz W. The design and analysis of computer experiments. London, UK: Springer Series in Statistics; 2003.

[21] Sacks J, Welch W, Mitchell T, Wynn H. Design and analysis of computer experiments. Stat Sci 1989;4(4):409–35.

[22] Xiong Y, Chen W, Appley D, Ding X. A non-stationary covariance-based kriging method for metamodelling in engineering design. Int J Numer Methods Eng 2006;71:733–56.

[23] DiazDelaO FA, Adhikari S. Structural dynamic analysis using Gaussian process emulators. Eng Comput 2010;27(5):580–605.

[24] DiazDelaO FA, Adhikari S. Gaussian process emulators for the stochastic finite element method. Int J Numer Methods Eng 2011;87(6):521–40.

[25] Hill R. A self-consistent mechanics of composite materials. J Mech Phys Solids 1965;13(4):213–22.

[26] Mandel J. Plasticite classique et viscoplasticite. In: CISM lecture notes. Udine, Italy: Springer-Verlag; 1971.

[27] de Souza Neto EA, Feijóo R. Variational foundations of large strain multi-scale solid constitutive models: kinematical formulation. In: Vaz M, Jr., de Souza Neto E, oz Rojas PM, editors. Advanced multi-scale material modelling: from classical to multi-scale techniques. Chichester: Wiley; 2010.

[28] de Souza Neto EA, Perić D, Owen DRJ. Computational methods for plasticity: theory and applications. Chichester: Wiley; 2008.

[29] Lemaitre J, Chaboche JL. Mechanics of solid materials. Cambridge: Cambridge University Press; 1990.

[30] Oakley J. Eliciting Gaussian process priors for complex computer codes. The Statistician 2002;51(1):81–97.

[31] O'Hagan A. Bayesian analysis of computer code outputs: a tutorial. Reliab Eng Syst Safety 2006;91(10–11):1290–300.

[32] Oakley JE, O'Hagan A. Probabilistic sensitivity analysis of complex models: a Bayesian approach. J Roy Stat Soc B 2004;66(3):751–69.

[33] Oakley J. Estimating percentiles of computer code outputs. Appl Stat 2004;53:83–93.

[34] Haylock R, O'Hagan A. Bayesian statistics, vol. 5. Oxford, UK: Oxford University Press; 1996 [Ch. On inference for outputs of computationally expensive algorithms with uncertainty on the inputs].

[35] O'Hagan A. Bayesian statistics, vol. 4. Cambridge, UK: Oxford University Press; 1992. pp. 345–363 [Ch. Some Bayesian numerical analysis].

[36] Haylock R. Bayesian inference about outputs of computationally expensive algorithms with uncertainty on the inputs. Ph.D. thesis, University of Nottingham, Nottingham, UK; 1996.

[37] Rougier J. Probabilistic inference for future climate using an ensemble of climate model evaluations. Climatic Change 2007;81(3):247–64.

[38] Oakley JE, O'Hagan A. Bayesian inference for the uncertainty distribution of computer model outputs. Biometrika 2002;89:769–84.

[39] de Souza Neto EA, Perić D, Dutko M, Owen DRJ. Design of simple low order finite elements for large strain analysis of nearly incompressible solids. Int J Solids Struct 1996;33:3277–96.

[40] Bastos LS, O'Hagan A. Diagnostics for Gaussian process emulators. Technometrics 2009;51(4):425–38.

[41] O'Hagan A. Kendall's advanced theory of statistics, vol. 2B. London: Arnold; 1994 [Ch. Bayesian Inference].

[42] Krzanowski W. Principles of multivariate analysis. Oxford, UK: Oxford University Press; 2000.